

Feasibility Study of Rapid Prototyping Using the Uniform Droplet Spray Process

by

Jennifer Hyunjong Shin

Submitted to the Department of Mechanical Engineering
in Partial Fulfillment of the Requirements for the Degree of

BACHELOR OF SCIENCE

at the

MASSACHUSETTS INSTITUTE OF TECHNOLOGY

May 1998

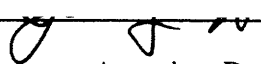
[June 1998]

© 1998 Massachusetts Institute of Technology
All Rights Reserved

Signature of Author:


Department of Mechanical Engineering
May 8, 1998

Certified by:


Jung-Hoon Chun
Associate Professor of Mechanical Engineering
Thesis Supervisor

Accepted by:


Derek Rowell
Professor of Mechanical Engineering
Chairman, Department Undergraduate Committee

JUN 30 1998

LIBRARIES

ARCHIVES

Feasibility Study of Rapid Prototyping Using the Uniform Droplet Spray Process

by

Jennifer Hyunjong Shin

Submitted to the Department of Mechanical Engineering
on May 8, 1998 in Partial Fulfillment of the Requirements for the Degree of
Bachelor of Science in Mechanical Engineering

ABSTRACT

This work studied the feasibility of rapid prototyping using the Uniform Droplet Spray (UDS) process. Straight and stable liquid metal jets are crucial requirements in the application of UDS to rapid prototyping. Methods to maintain the jet straight and stable were developed. Hardware improvements include an auxiliary orifice mounting fixture and a new crucible bottom with a tightly-fitting orifice-pocket. A droplet trajectory controller, including deflection plates and a pulse provider to a charging plate, was developed to precisely deliver droplets for deposition. The degree of separation between deflected and undeflected streams of droplets was modeled and the prediction was compared with experimental results. This comparison revealed that the degree of actual deflection was approximately twice as high as the predicted value. Using the trajectory controller, deposition was conducted using pure tin (Sn) with droplet impact conditions of velocity and liquid fraction of 4.5 m/s and 97%, respectively. The deposition frequency was varied in the experiment to study its effects on deposit shapes. A low frequency deposition at 57Hz produced a vertical pillar, whereas a high frequency deposition at 574Hz resulted in a large drop.

Thesis Supervisor:
Dr. Jung-Hoon Chun
Associate Professor of Mechanical Engineering

Acknowledgments

First of all, I would like to thank Professor Jung-Hoon Chun, my thesis advisor, for providing me with this opportunity to write this thesis under his guidance. Special thanks to Professor C. Forbes Dewey, my academic advisor, for his consistent encouragement. Other faculty members of MIT, especially Prof. Lallit Anand, Simone Hochgreb, Gene Brown, Deborah Kruzel, and L. Mahadevan, made my undergraduate life so fruitful.

I would also like to thank everyone in the Droplet-Based Manufacturing (DBM) laboratory for their help. My sincere gratitude to Mr. Ho-Young Kim for his care and help above any point I would have asked of him throughout a year as a supervisor. Thank you, Jeanie Cherng, Sukyoung Chey, and Juan-Carlos Rocha, for teaching and helping me in so many ways.

With warmest regards and appreciation to my dearest friends, Jane Lah, Heather Koh, Joyce Hahn, and Sohee Shin, for their encouragement and support for last 4 years. Special thanks to my sister-like roommate Sung Sim Park who provided me with late night snacks and a warm care throughout my senior year.

Especially, I would like to acknowledge my parents in Korea with my greatest thanks as all of my accomplishments have always been for them. I also thank my four sisters who always prayed for me and gave me the selfless love. Special thanks to my four brothers-in-law, nephews and nieces for their love and smiles.

God, I thank you so much for everything that happened to me. Watch me grow in you with your greatest love.

Table of Contents

Title Page	1
Abstract	2
Acknowledgments	3
Table of Contents	4
List of Tables	6
List of Figures	7
1 INTRODUCTION	8
1.1 Background	8
1.2 Overview of the Investigation	8
2 STRAIGHT AND STABLE STREAM	11
2.1 Orifice Mounting Device	11
2.2 Crucible Bottom with a Tight Orifice-Pocket	12
3 CONTROL OF DROPLET TRAJECTORY AND DEPOSITION RATE	14
3.1 Principles of Deflection	14
3.2 Theoretical Prediction	15
3.3 Experimental Results and Comparison with Theoretical Prediction	18
4 DEPOSITION OF MOLTEN METAL DROPLETS	22
4.1 Introduction	22
4.2 Velocity of Uncharged Droplets	22
4.2.1 Drag Coefficient of a Droplet in an Aligned Stream	23
4.2.2 Drag Coefficient of Individual Droplets	24
4.2.3 Simulation of Droplet Velocity	24
4.3 Thermal States of Uncharged Droplets	24
4.3.1 Energy Balance	24
4.3.2 Simulation of Droplet Thermal States	25
4.4 Deposition Experiment	25
4.4.1 Experimental Procedure	25
4.4.2 Experimental Results	26

5 CONCLUSIONS

28

BIBLIOGRAPHY

29

List of Tables

Table 2.1	Experimental conditions of droplet sprays for the straightness and jumpiness tests with a new crucible bottom	13
Table 4.1	Initial condition of pure tin droplet spray for the deposition experiment	26

List of Figures

Figure 1.1	Schematic Diagram of the UDS Process	9
Figure 2.1	Old Crucible Bottom with a Mounted Orifice	11
Figure 2.2	Schematic of an Orifice Mounting Fixture	12
Figure 2.3	Measures of Straightness and Jumpiness	13
Figure 3.1	Droplet Trajectory Controller	15
Figure 3.2	Schematic of a Deflection System	16
Figure 3.3	Deflected distance vs. Charging voltage (δ vs. V_{ch})	17
Figure 3.4	Deflected distance v. Deflection voltage (δ vs. V_d)	18
Figure 3.5	Separated Droplet Streams Due to Deflection	19
Figure 3.6	Comparison between the experimental results and the theoretical prediction of δ vs. V_d at $V_{ch} = 400$ V	19
Figure 3.7	Comparison between the experimental results and the theoretical prediction of δ vs. V_d at $V_{ch} = 350$ V	20
Figure 3.8	Comparison between the experimental results and the theoretical prediction of δ vs. V_d at $V_{ch} = 300$ V	20
Figure 4.1	Flight of Droplets	23
Figure 4.3	Deposits at two Different Frequencies	27

Chapter 1 INTRODUCTION

1.1 Background

Rapid prototyping is a process used to fabricate three dimensional (3-D) objects directly from CAD information. It reduces design and manufacturing steps in product development and thus is highly efficient. There are several methods of rapid prototyping, such as stereolithography, selective laser sintering, fused deposition modeling, and 3-D printing. These methods have the common shortcomings of multi-step processes and of poor mechanical strength.

Rapid prototyping using the Uniform Droplet Spray (UDS) process, which was developed at MIT (Chen et al., 1996), can fabricate objects with good mechanical strength in a single step. The UDS process is a novel method of Droplet-Based Manufacturing (DBM) which generates droplets of a uniform size. Figure 1.1 is a schematic diagram of the UDS process. Metal in a crucible is melted by a heater and ejected through an orifice by pressure applied from an inert gas supply. The ejected molten metal forms a laminar jet, which is vibrated by a piezoelectric transducer at a specified frequency. The disturbance from the vibration grows until the jet breaks up into a stream of uniform droplets. During the break-up process, each droplet is electrically charged by a direct-current (DC) voltage applied at a charging plate. The charged droplets repel each other, preventing merging.

The UDS process can construct 3-D objects droplet by droplet as a computer controlled substrate moves according to the CAD design. The uniform molten metal droplets are densely deposited on a substrate and rapidly solidified to consolidate into compact and strong deposits. It is essential to gain precise control of droplet trajectories and deposition rates to apply the UDS process to rapid prototyping. These elements determine the accuracy of the resulting part geometry. However, as described above, droplets are electrically charged at break-up and scatter due to electrical repulsion. This thesis develops a method to precisely deliver droplets to a desired location. The method selectively deflects droplets using the electrical charge imposed on them. This method can also control the deposition rate of droplets.

1.2 Overview of the Investigation

The goal of this study is to examine the feasibility of rapid prototyping using the UDS process. The primary condition required in the application of the UDS process to

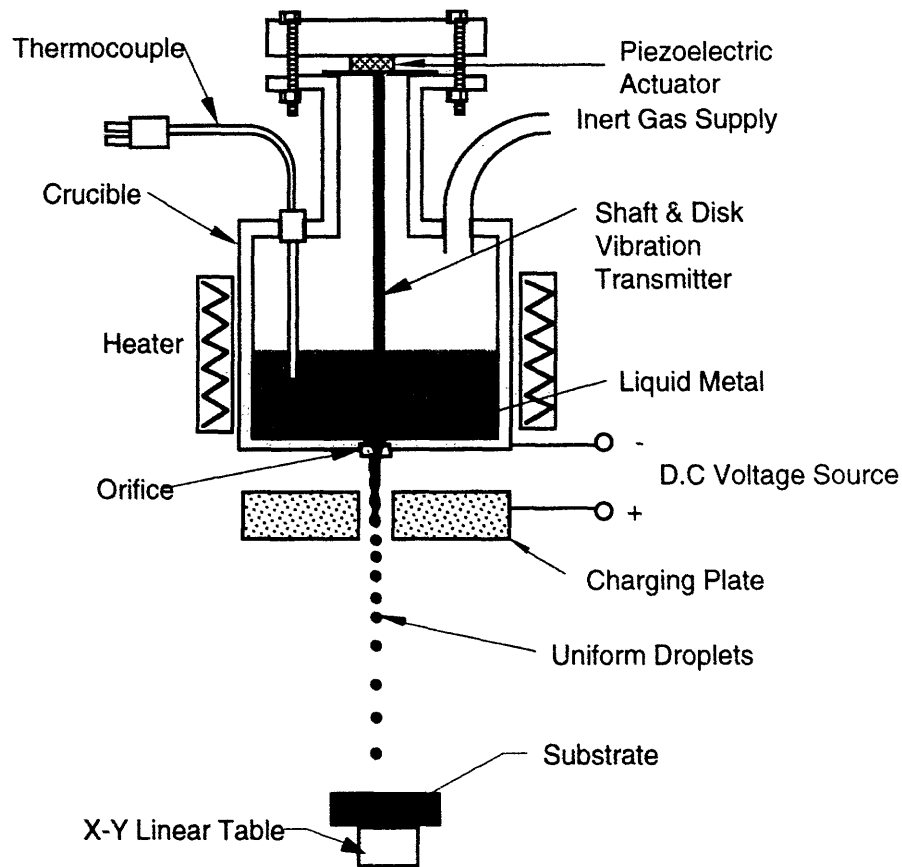


Figure 1.1 Schematic Diagram of the UDS Process

rapid prototyping is to obtain a straight stream of droplets from a nozzle. In view of this requirement, an orifice mounting device and a newly designed crucible bottom were tested. Once a straight stream had been achieved, the feasibility of rapid prototyping was studied by employing the deflection system. The deflection system, a pair of deflection plates and a pulse signal provider to a charging plate, can selectively deflect droplets and thus control droplet trajectory. The influence of charging and deflecting voltages on the degree of deflection was predicted and compared with experimental results. Lastly, the deflection frequency was varied to change the deposition rate and accordingly, to generate different shapes of deposit. This study provides an initial look at applying the UDS process to the field of rapid prototyping.

Chapter 1 describes the background and objectives of this study. Chapter 2 explains methods used to generate a straight stream of droplets. Chapter 3 details both the theoretical and the experimental study of the deflection system. The relationship between the voltage (of both charging and deflection) and the degree of deflection is theoretically predicted and compared with experimental results. In Chapter 4, the velocity and thermal

states of droplets are simulated to predict the impact conditions of droplets. Results of deposition, conducted at different deflection frequencies, are presented to verify the feasibility of rapid prototyping using the UDS process. Conclusions are presented in Chapter 5.

Chapter 2 STRAIGHT AND STABLE STREAM

A primary condition required in the application of the UDS process to rapid prototyping is a straight and stable stream of droplets. It has been frequently noticed that the stream tends to be crooked and jumpy during a run. The crookedness and the jumpiness of the stream are caused by oxides or impurities in the molten metal around the nozzle and by a poorly mounted orifice. A spray chamber should contain as little oxygen as possible, and a jetting device should be maintained free of contamination to reduce oxides and impurities in molten metal. The original orifice mounting scheme had problems. Since the size of an orifice is very small (approximately 2mm in outer diameter), it is difficult to mount the orifice flat and to fix it stably in a pocket whose opening was approximately 3 mm in diameter (Figure 2.1). The mounting adhesive for the orifice cannot fill the gap completely and evenly, which causes the orifice to be slanted and to wobble inside the pocket.

2.1 Orifice Mounting Device

A new method of mounting an orifice with an auxiliary orifice mounting fixture was devised to solve the problem of orifice mounting. As shown in Figure 2.2, a 3.9mm diameter bolt on the top of the device was used to press the fixer rod down on the orifice during orifice mounting and cement curing. This scheme ensures that the orifice is kept straight. However, the gap between the orifice and the pocket wall was still present and the cement was unable to fill the gap completely. Consequently, the stream became less crooked but remained jumpy.

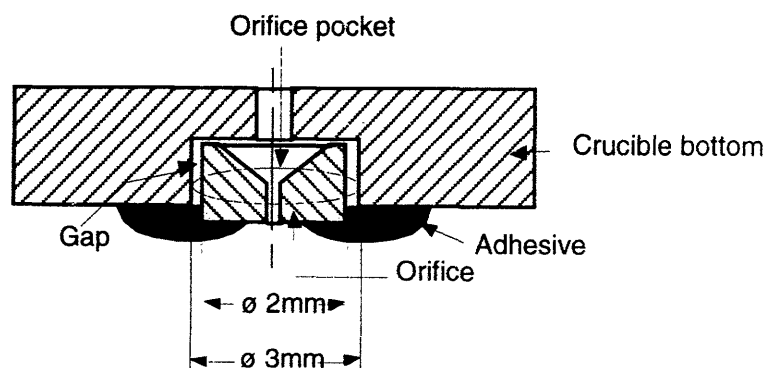


Figure 2.1 Old Crucible Bottom with a Mounted Orifice

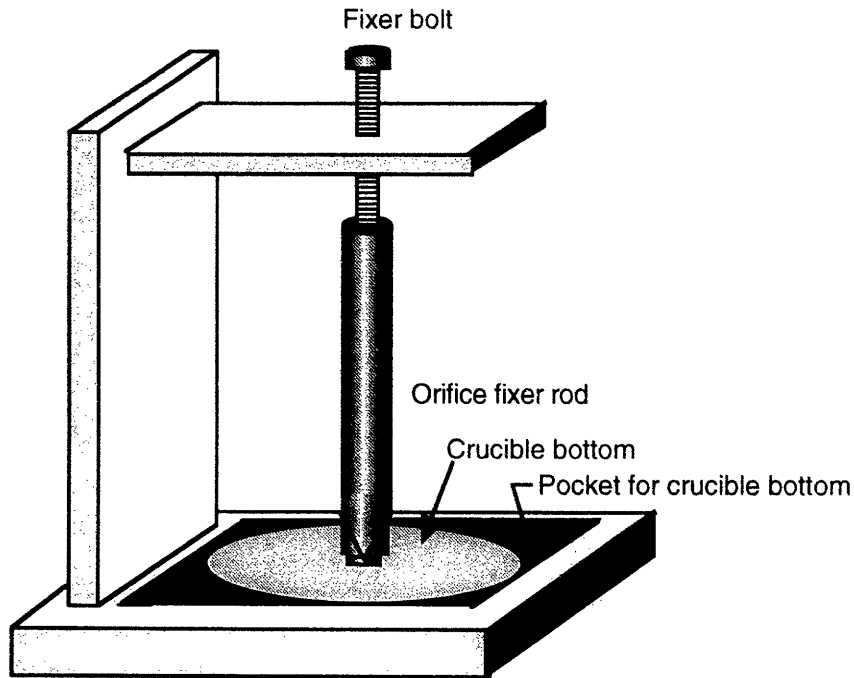


Figure 2.2 Schematic of an Orifice Mounting Fixture

2.2 Crucible Bottom with a Tight Orifice-Pocket

A new method was needed to hold the orifice stably as well as straight. A crucible bottom was remachined to reduce the size of the orifice pocket, so that an orifice could be tightly fit in the orifice pocket. This orifice was expected to stay straight and stable during both a curing process and an experiment. For every experiment with a new crucible bottom, the jumpiness and straightness of the streams were measured. The angle α was employed as a measure of straightness (See Figure 2.3): this angle α can be rewritten as $\alpha = d_c/L$ where L is the length from the orifice to the bottom of the plates in Figure 2.3, and d_c is the distance from the stream to the centerline of the plates at the bottom of the plate, assuming that a straight stream travels along the centerline between the plates. As a measure of jumpiness, another angle β , where $\beta = \beta_1 + \beta_2$, was employed. As indicated in Figure 2.3, the angle β is the sum of $\tan^{-1}(S_1/L)$ and $\tan^{-1}(S_2/L)$. Since the angle β is very small here, $\tan\beta$ can be approximated as β . Therefore, the jumpiness measure β can be written as $\beta = (S_1 + S_2)/L$.

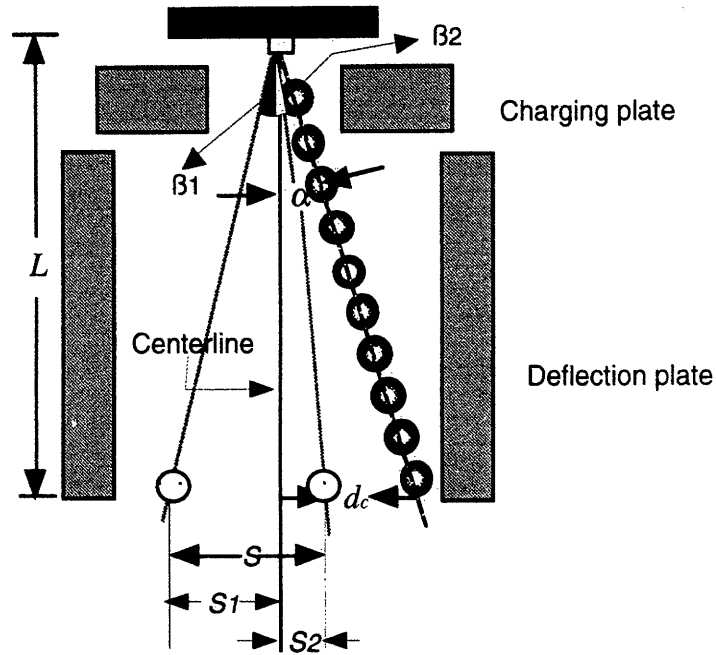


Figure 2.3 Measures of Straightness and Jumpiness

According to the measurement results obtained from 10 runs whose conditions are shown in Table 2.1, the average crookedness of the stream with an orifice of 150 μm diameter, was 0.14° with a standard deviation of 0.38° . The average jumpiness was 0.005° with a standard deviation of 0.009° . With a 100 μm diameter orifice, the average crookedness was 5° with a standard deviation of 6.2° . Its jumpiness was 0.005° with a standard deviation of 0.009° . Although it was still difficult to generate a straight stream with a 100 μm diameter orifice, overall, significant improvement in both crookedness and jumpiness was achieved by using a crucible bottom with a tightly fitting fit orifice-pocket.

Table 2.1 Experimental conditions of droplet sprays for the straightness and jumpiness tests with a new crucible bottom

Exp #	1	2
Orifice diameter (μm)	100	150
Ejection Pressure (kPa)	138	103
Melt material	pure tin	pure tin
Melt temperature (K)	573	573
Repetition (times)	2	8

Chapter 3 CONTROL OF DROPLET TRAJECTORY AND DEPOSITION RATE

3.1 Principles of Deflection

Having achieved a straight and stable stream of droplets, it is now necessary to develop a new method to precisely deliver the droplets to a desired location. As described in Chapter 1, droplets become electrically charged as they pass between a charging plate, and the charged droplets scatter due to electrical repulsion. The scattered droplets make a precise geometry difficult in rapid prototyping. In addition, it is difficult to control the droplet deposition rate, which is determined by droplet generation frequency. A droplet trajectory controller was developed to overcome these problems,. Figure 3.1 shows the schematic of the controller. The controller includes deflection plates located under the charging plates and a pulse signal provider which sends pulse signals to the charging plate. The charging plate is connected to a voltage controller which provides the plate with a constant voltage signal (on the order of 400V) with short (100 μ s) zero-voltage pulses periodically. One deflection plate is connected to another high voltage source, the other plate to the ground. Hence, a constant electric field is maintained in a horizontal direction between the deflection plates.

Due to the periodic zero-voltage pulses in the charging voltage, only those droplets generated when the charging plate is on (the high voltage is supplied) are electrically charged as they pass through the charging region. Those droplets generated when the charging plate is off (zero-voltage pulse is supplied) remain uncharged. When droplets pass the deflection plate downstream, only the charged droplets are affected by the electric field and thus deflected off the centerline. The uncharged droplets are not affected by the electric field and so travel straight down to a desired location for deposition.

Both the charging voltage and the deflection voltage can be varied to influence the degree of deflection of the charged droplets. The number of straight-falling droplets can be controlled by changing the frequency of the zero-voltage pulses. This change in deposition rate alters the deposition characteristics (See Chapter 4).

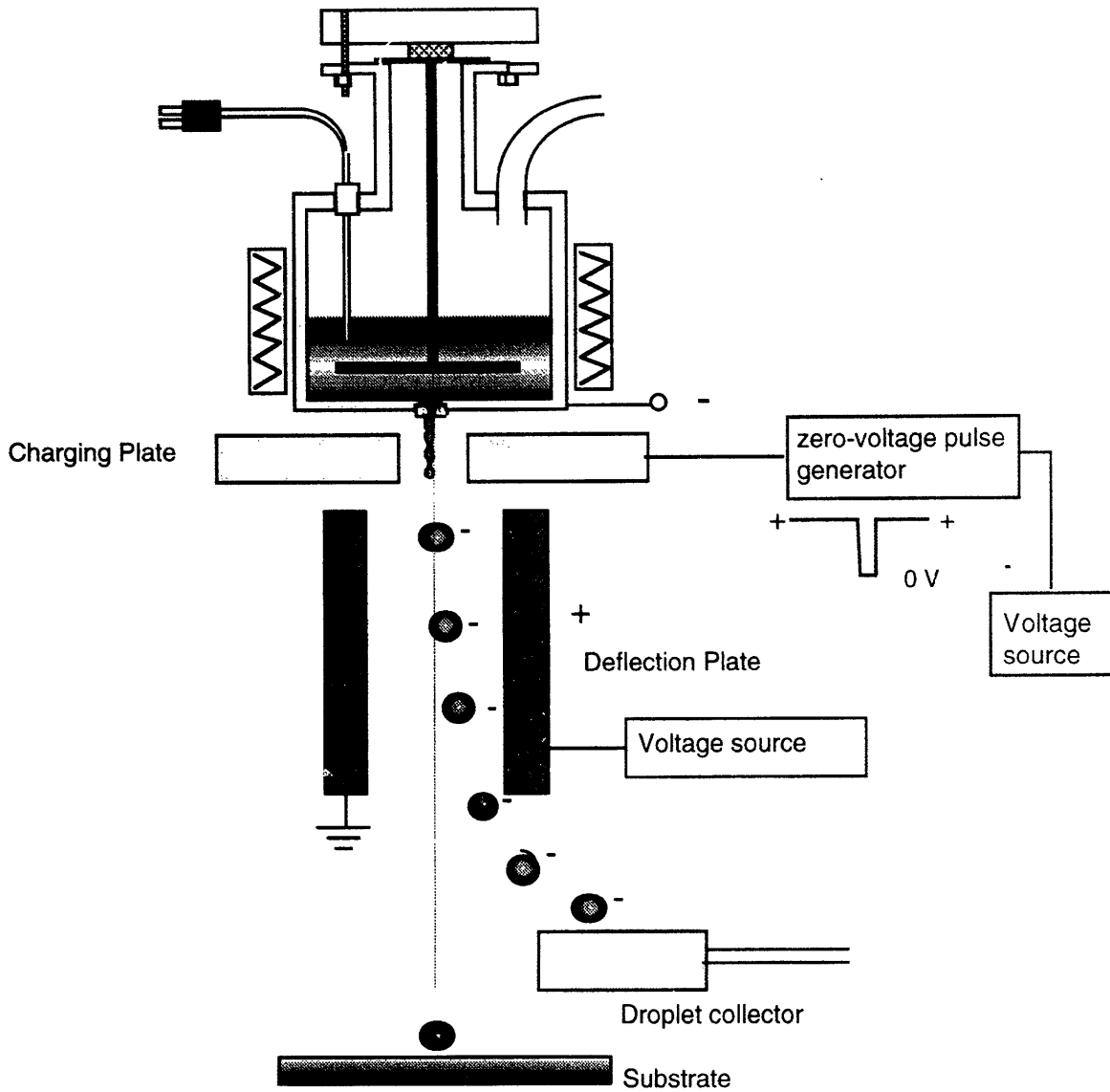


Figure 3.1 Droplet Trajectory Controller

3.2 Theoretical Prediction

Figure 3.2 shows the schematic of a deflection system. The deflected distance, δ , of the charged droplets as they emerge from the deflection region can be calculated to be:

$$\delta = \frac{1}{2} a t_{\delta}^2 \quad (3.1)$$

where a is the horizontal acceleration of the droplet and t_{δ} is the time the droplet takes to travel down the length of the deflection plates ℓ_d .

When the electric potential difference V_d is applied between the deflection plates, there is a horizontal electrical field with magnitude $E = V_d/d$ between the plates where d is the distance between the deflection plates. A constant horizontal force with magnitude qE then acts on the charged droplets, and their horizontal acceleration a can be expressed as:

$$a = \frac{qE}{m} = \frac{qV_d}{md} \quad (3.2)$$

where m is the mass of a droplet. The mass of a droplet is given by $m = \pi D^3 \rho / 6$ where D being the droplet diameter given as $D = (3d_j^2 v_j / 2f)^{1/3}$ where d_j is the jet diameter, f is the droplet generation frequency, and v_j is the jet velocity. The amount of charge induced in each droplet, q , is (Passow 1992):

$$q = \frac{2\pi\epsilon_0 v V_{ch}}{\ln(d_c/d_j) f} \quad (3.3)$$

where ϵ_0 is the permittivity of free space, V_{ch} is the charging voltage, and d_c is the diameter of a charging ring opening.

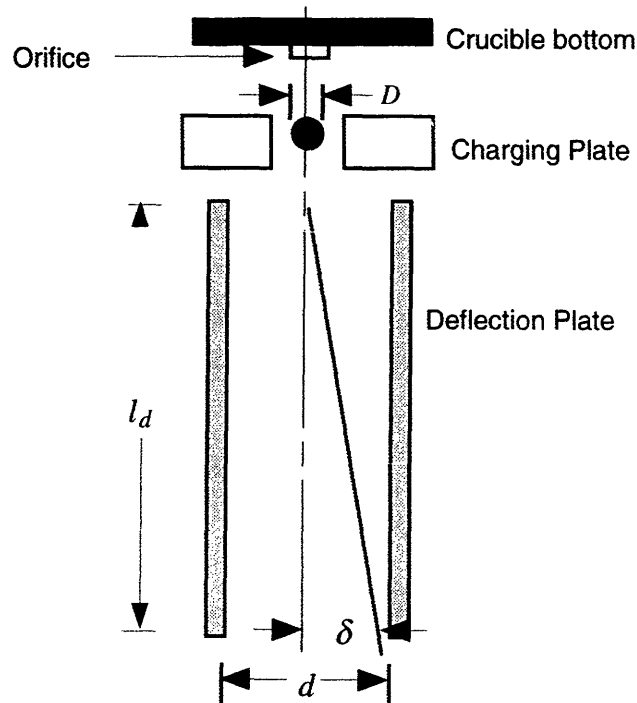


Figure 3.2 Schematic of a Deflection System

The time t_δ in Eq. (3.1), which is required for the charged droplets to travel the length l_d , can be obtained by:

$$t_\delta = \frac{l_d}{v} \quad (3.4)$$

where the velocity v was assumed to be constant.

Finally, by substituting the expressions for a and t_δ given by Eq. (3.2), (3.3), and (3.4) into Eq. (3.1), the equation for deflection distance, δ , can be obtained:

$$\delta = \left(\frac{4\epsilon_0 l^2}{\rho d_j^2 v^2 \ln(d_c/d_j) d} \right) V_{ch} V_d \quad (3.5)$$

The deflection distance δ is proportional to both the deflecting voltage V_d and the charging voltage V_{ch} . Figure 3.3 and 3.4 are the theoretical prediction plots of δ vs. V_{ch} and δ vs. V_d , respectively. It is noteworthy that the deflection is independent of the droplet generation frequency f .

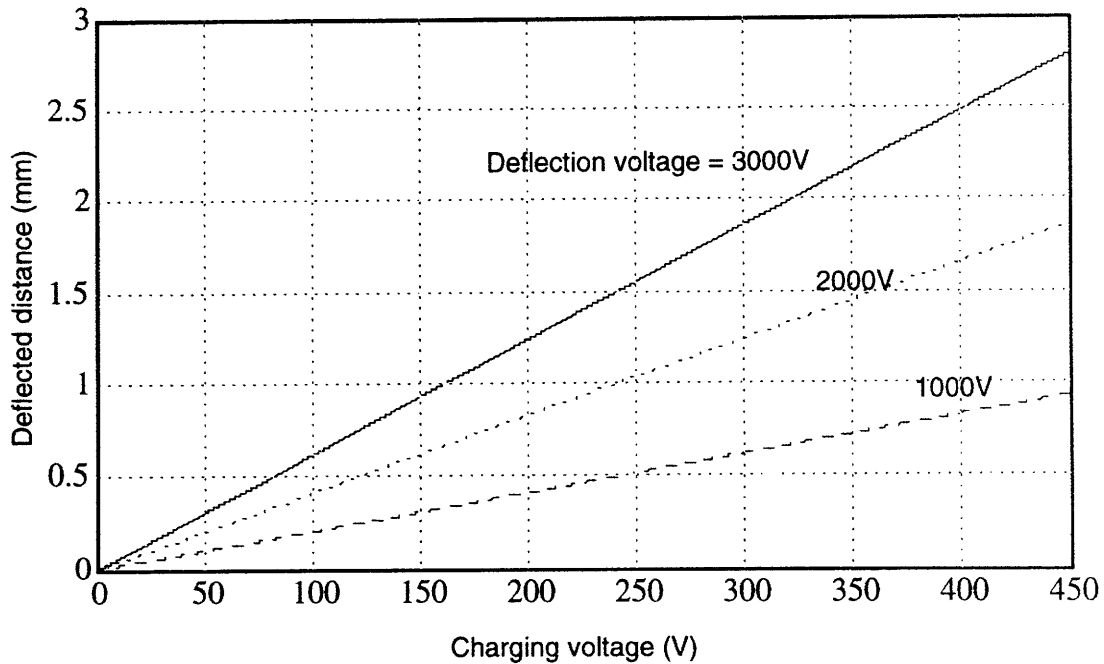


Figure 3.3 Deflected distance vs. Charging voltage (δ vs. V_{ch})

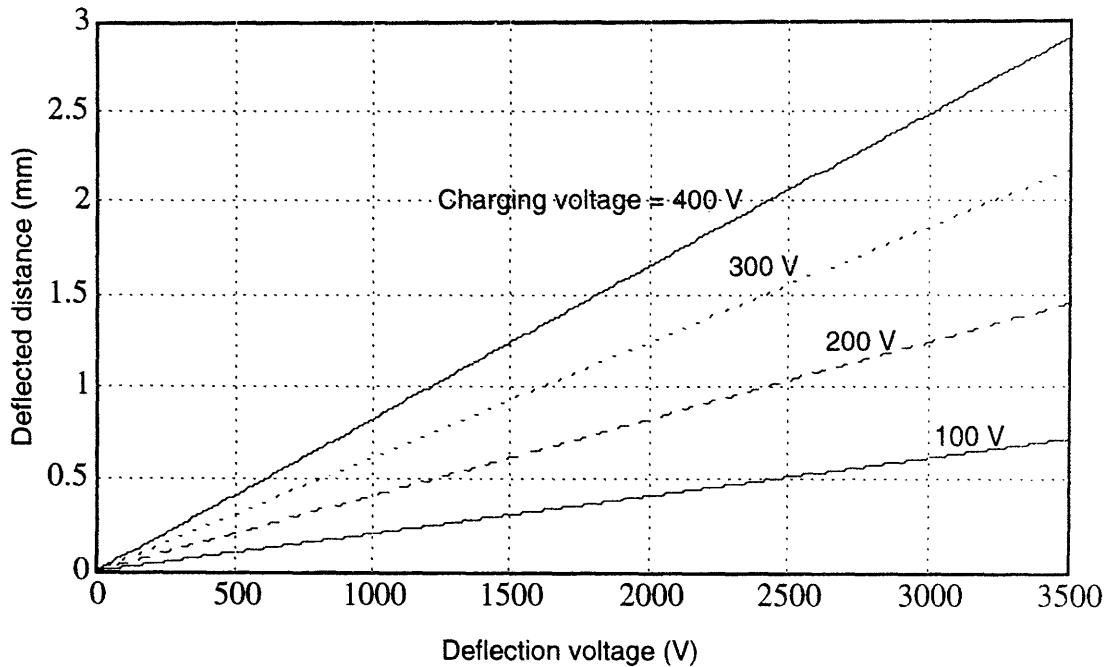


Figure 3.4 Deflected distance v. Deflection voltage (δ vs. V_d)

3.3 Experimental Results and Comparison with Theoretical Prediction

Using the apparatus shown in Figure 3.1, the deflected distance δ was measured while changing the charging voltage V_{ch} and the deflection voltage V_d . In addition, the frequency of zero-voltage pulse was varied at fixed V_{ch} and V_d to measure the sensitivity of δ to the frequency.¹

Figure 3.5 shows the stream of deflected droplets at the end of the deflection region. Three straight-falling droplets in the middle of deflection plates are uncharged droplets used in deposition. The charging voltage was 390V² and the deflection voltage was 3kV in this figure. Other experimental conditions are the same as Exp. #2 of Table 2.1. As predicted by Eq.(3.5), when either the deflection voltage or the charging voltage was increased, the deflected distance increased. Deflected distances δ at different charging and deflection voltages were measured from the recorded data and compared with theoretical prediction (Figures 3.6, 3.7, and 3.8). It is observed that there is a significant discrepancy between the experimental results and the theoretical prediction. The deflected distance of the experimental results is approximately twice that of the theoretical prediction.

¹ It is again noted that the degree of deflection is independent of droplet generation frequency.

² 400 V is the maximum amount of charging voltage that can be used due to the limit of a power transistor in the pulse provider

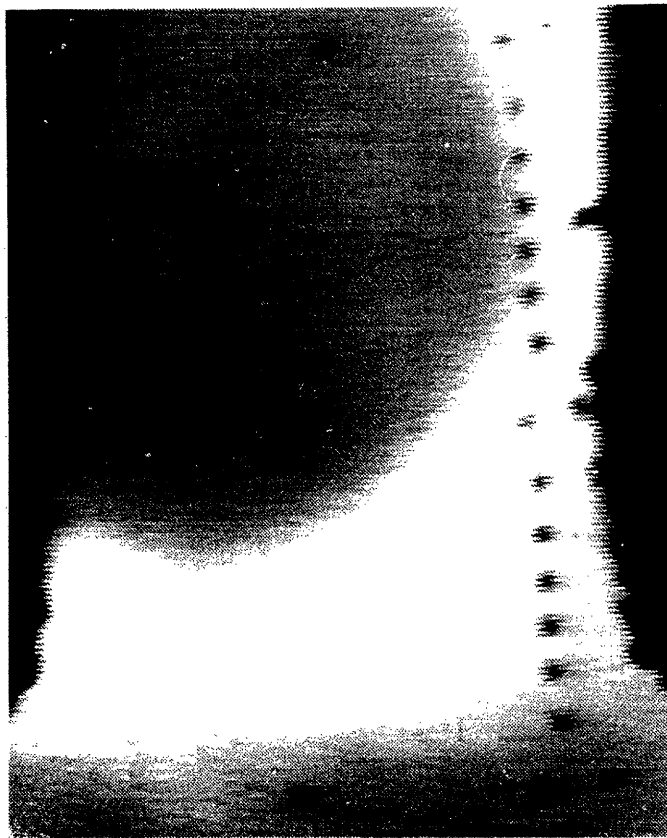


Figure 3.5 Separated Droplet Streams Due to Deflection

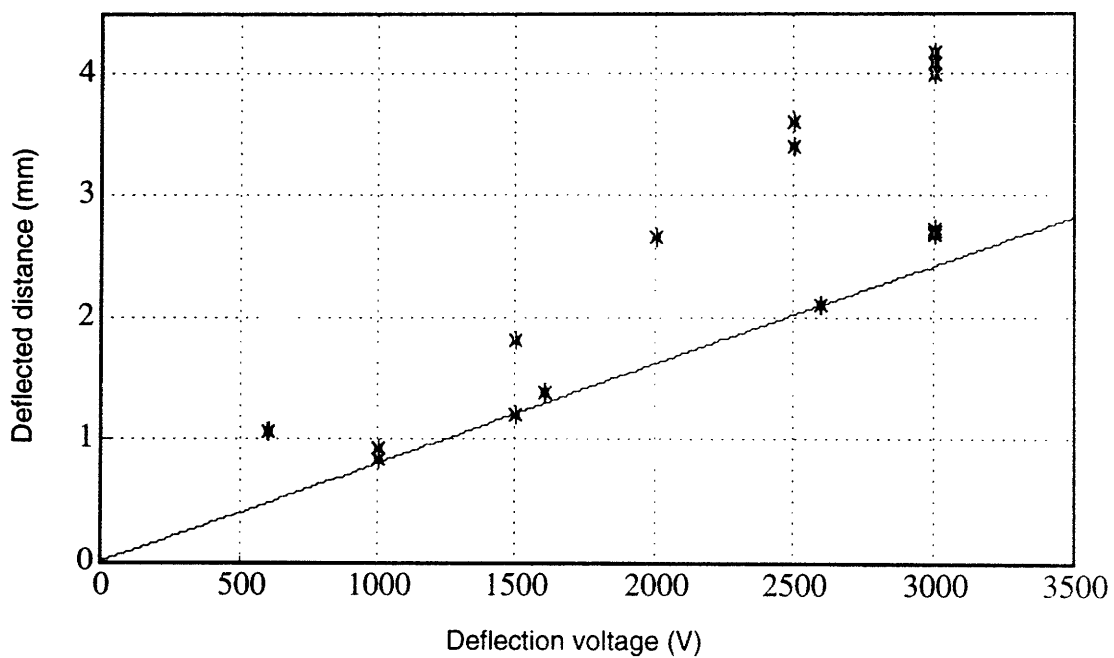


Figure 3.6 Comparison between the experimental results and the theoretical prediction of δ vs. V_d at $V_{ch} = 400$ V

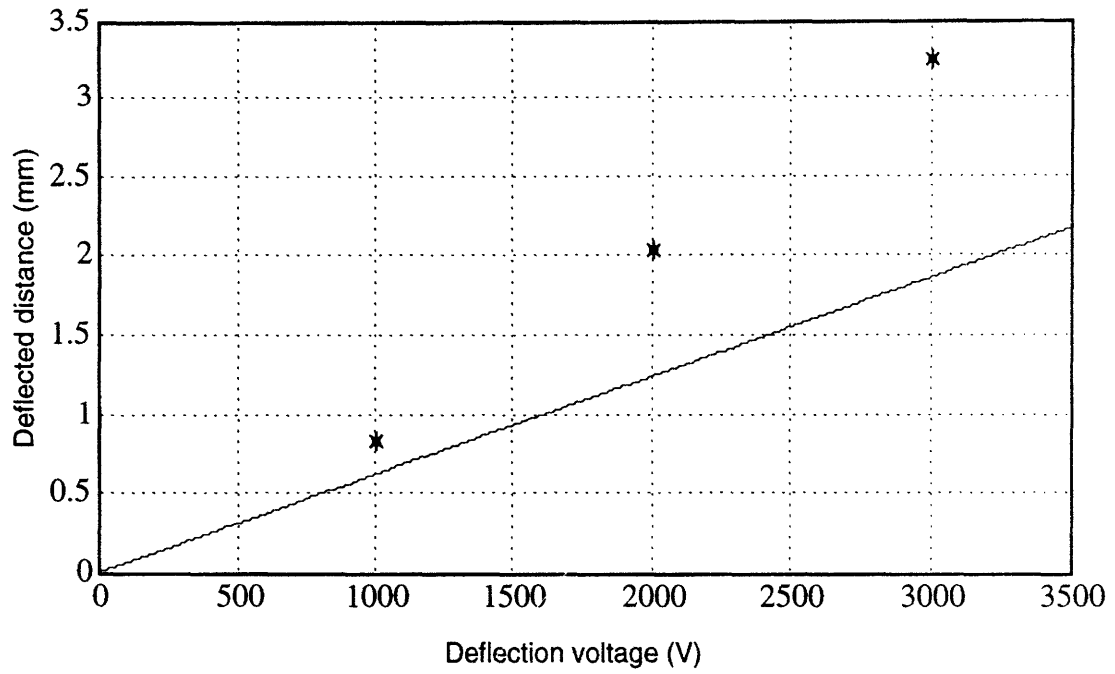


Figure 3.7 Comparison between the experimental results and the theoretical prediction of δ vs. V_d at $V_{ch} = 350$ V

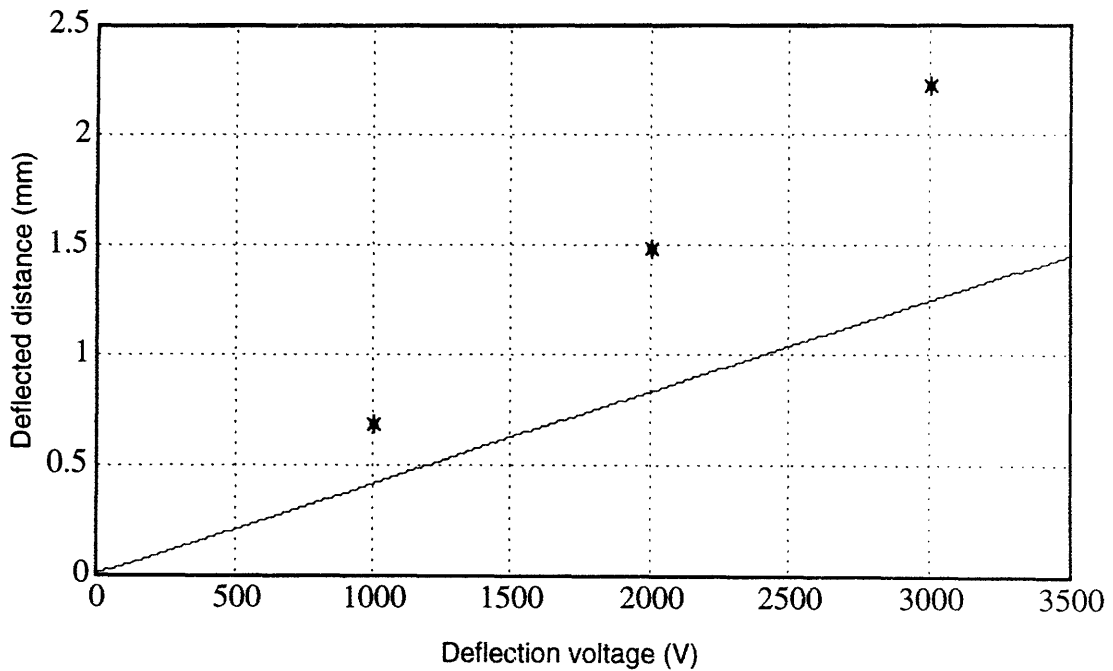


Figure 3.8 Comparison between the experimental results and the theoretical prediction of δ vs. V_d at $V_{ch} = 300$ V

Several factors may contribute to this discrepancy. First, in Eq.3-3 for the electric charge of a droplet q , a stream of droplets was assumed to travel along the centerline of the charging ring. During an experiment, however, the center of the orifice and the center of the charging ring may not coincide. Abel (1993) verified that the value of electric charge q on a droplet increases as the distance between the centerline and the liquid jet increases. Therefore, the predicted value of q is always the minimum value of q that a droplet may attain. As a consequence, the actual horizontal electrical force is always larger than the predicted value, as is the actual horizontal acceleration a (See Eq.(2)). A higher acceleration a results in a greater deflected distance δ .

Secondly, an error inherent in the measurement techniques of the deflected distance may contribute to the discrepancy. Since the size of the droplets is on the order of $100\ \mu\text{m}$ and the spray is performed inside an inert gas chamber, a direct measurement of deflected distance is impossible. An indirect measurement is used, in which a view of droplets of interest is magnified and captured by a CCD camera (Techni-Quip TQ/V), recorded by a VCR (Sony SLV-495), and replayed on a monitor (Sony PVM-1390) on which the actual measurement is conducted. This procedure has a precision limit, and a similar error is reported by Yim (1996). Since the deflected distance δ is on the order of 1mm , any small error in measurement can result in a large discrepancy.

Chapter 4 DEPOSITION OF MOLTEN METAL DROPLETS

4.1 Introduction

The deposit shape of molten droplets greatly depends on the frequency of zero-voltage pulses which affect the deposition rate of straight-falling droplets. In addition, other factors such as velocity, temperature, liquid fraction of droplets at the moment of impact, and substrate conditions affect deposit shape. In this work, different shapes of deposit were produced by changing the deposition rate while keeping the other conditions identical. The velocity and thermal states of deposited droplets were numerically simulated to evaluate the deposition conditions.

4.2 Velocity of Uncharged Droplets

The velocity of uncharged droplets can be predicted by balancing the force acting on them, i.e. gravitational force and drag force; $m\ddot{\mathbf{r}} = m\mathbf{g} + \mathbf{F}_d$, where $\ddot{\mathbf{r}}$ is the acceleration of a droplet, m the mass of a droplet, and \mathbf{F}_d is the drag force:

$$\mathbf{F}_d = C_d \left(\frac{\pi}{4} D^2 \right) \left(\frac{1}{2} \rho_g |\dot{\mathbf{r}}| \dot{\mathbf{r}} \right) \quad (4.1)$$

where C_d is the drag coefficient, D the diameter of a droplet, ρ_g the density of the gas, and $\dot{\mathbf{r}}$ the velocity of a droplet. Drag force is determined by flow conditions surrounding the droplets. Uncharged droplets experience two different flow conditions as they travel down. Before they enter the deflection region, they are members of an aligned stream of both charged and uncharged droplets. On entering the deflection region, the charged droplets deflect off the centerline while the uncharged ones keep falling along the centerline as individual droplets. Due to wake effects, the drag force acting on a droplet in an aligned stream is less than that on an individual droplet (Mulholland et al., 1988). Therefore, prior to entering the deflection region, a drag coefficient for an aligned stream should be used (See 4.2.1). On the other hand, C_d for an individual droplet should be used after entering the deflection region (See 4.2.2).

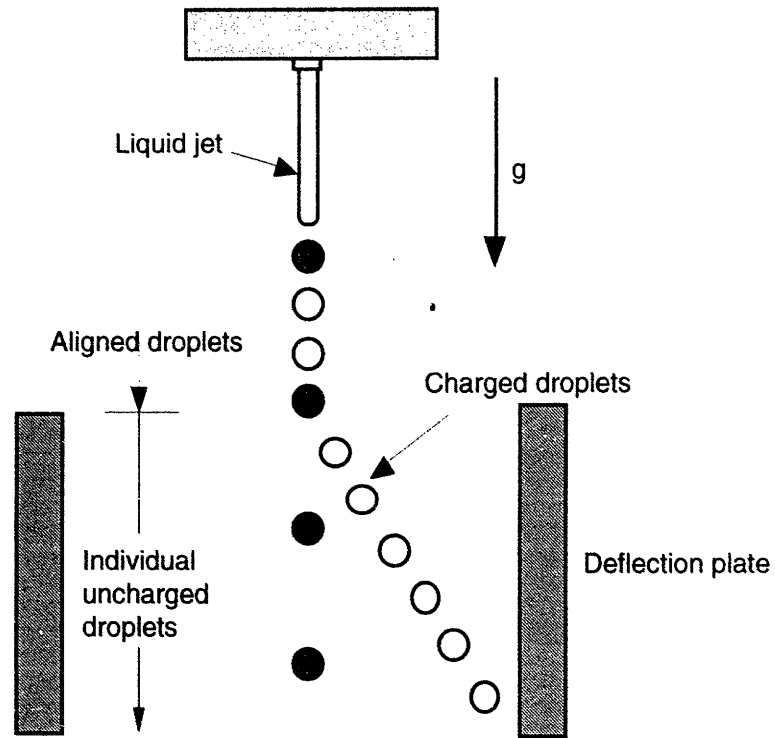


Figure 4.1 Flight of Droplets

4.2.1 Drag Coefficient of a Droplet in an Aligned Stream

The drag coefficient of a droplet in a train of droplets is a function of a spacing between droplets and Reynolds number, Re :

$$Re = \frac{\rho_g v d}{\mu_g} \quad (4.2)$$

where μ_g is the viscosity of surrounding gas. Mulholland et al. (1988) assumes that the drag coefficient of droplets in an aligned stream, C_D^a , could be correlated as follows:

$$\left[C_D^a(Re, L/D) \right]^{-n} = \left[C_D^0(Re, L/D) \right]^{-n} + \left[C_D^\infty(Re) \right]^{-n} \quad (4.3)$$

where L is the spacing between two droplets, C_D^0 the asymptotic form for C_D^a as $L/D \rightarrow 1$, C_D^∞ the drag coefficient for isolated sphere, and n is the empirical parameter ($n=0.678$). C_D^0 is defined in this case as:

$$C_D^0(Re, L/D) = C_D^{0'}(Re) + aRe^{-1}(L/D - 1) \quad (4.4)$$

where $C_D^{0'}$ is the drag coefficient when $L/D=1$, and a is the empirical parameter ($a = 43.0$). $C_D^{0'}$ is given as follows:

$$\left[C_D^{0'}(Re) \right]^{-n} = \left[C_{rod}(Re) \right]^{-n} - \left[C_D^\infty(Re) \right]^{-n} \quad (4.5)$$

where C_{rod} is the drag coefficient of a long rod, $C_{rod}(Re) = 0.755/Re$. The drag coefficient, C_d^∞ , of an individual droplet is: (Mathur et al., 1989):

$$C_d^\infty(Re) = 0.28 + \frac{6}{\sqrt{Re}} + \frac{21}{Re} \quad (4.6)$$

4.2.2 Drag Coefficient of Individual Droplets

The drag coefficient described above is for droplets in an aligned stream. When droplets enter the deflection region, those uncharged droplets in the deflection region behave differently. The distance between two adjacent uncharged droplets is very large compared to the droplet diameter and thus the drag coefficient for a single sphere can be used. The drag coefficient for a single sphere was given by Eq (4.6).

4.2.3 Simulation of Droplet Velocity

Numerical simulation predicts the velocity of uncharged droplets. Using the input conditions of a spray: namely orifice size, charging voltage, and vibration frequency, the velocity is calculated based on force balance on a droplet. The initial jet velocity can be deduced by measuring the mass flow rate during spray (Kim, 1998).

4.3 Thermal States of Uncharged Droplets

4.3.1 Energy Balance

Thermal states of droplets can be obtained by considering heat transfer between a traveling droplet and surrounding gas. The rate of heat transfer can be expressed, ignoring radiation, as:

$$mC_p(dT_d/dt) = -hA(T_d - T_g) \quad (4.9)$$

where h is the convection heat transfer coefficient, A is the droplet surface area, T_d is the temperature of the droplet¹, and T_g is the gas temperature. The convection heat transfer coefficient h depends on surrounding flow conditions as a drag coefficient C_D does. Therefore, the heat transfer coefficient h should be obtained separately in two regions prior to and after the entering the deflection region. The heat transfer coefficient for a droplet in an aligned stream was modeled by Passow (1992). For an individual droplet, h is given by (Incropera and DeWitt, 1990):

$$h = \frac{k}{D} \left(2 + 0.6\text{Re}_d^{1/2} \text{Pr}^{1/3} \right) \quad (4.10)$$

where Pr is the Prandtl number of the surrounding gas.

4.3.2 Simulation of Droplet Thermal States

Numerical simulation predicts the temperature of uncharged droplets. Using the velocity simulation from Section 4.2.3, h can be calculated in both regions (before and after entering the deflection region). In the simulation, a finite difference method is employed to evaluate T_d (Kim, 1998).

4.4 Deposition Experiment

4.4.1 Experimental Procedure

Having successfully achieved a straight stream and a selective deflection of droplets, deposition itself can be addressed. This deposition serves as the feasibility test for rapid prototyping using the UDS process with the deflection system. The same apparatus is used as in Section 3.1, but with a substrate for deposition. Glass substrates 0.245 m below the deflection plates collected uncharged droplets. A gutter between the deflection plates and the substrate collected deflected droplets. The frequency of the zero-

¹ It is assumed that the temperature inside a droplet is uniform since the Biot number, $\text{Bi} = hd/k$, where d is a droplet diameter and k is the conductivity of the droplet, is very small ($\text{Bi} \ll 1$)

voltage pulse was changed to control the number of uncharged droplets and thus to investigate the effects of deposition rate on deposition morphology.

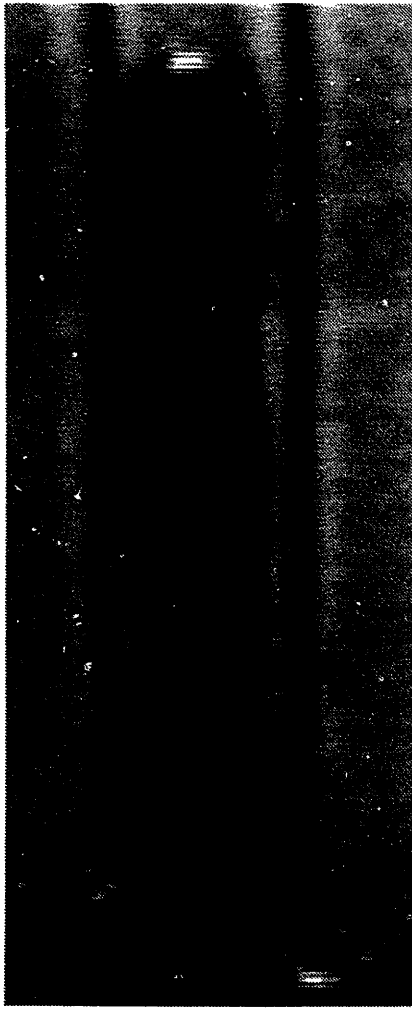
4.4.2 Experimental Results

Figures 4.3 (a) and (b) show deposits produced with the deposition frequency of 57 Hz and 574 Hz, respectively. The operating conditions of the droplet generator in this deposition process are listed in Table 4-1. The mass flow rate of the molten tin jet was 5.69×10^{-4} kg/s. The initial droplet velocity was 4.6 m/s and the droplet diameter, according to Table 4.1, was 150 μm . The substrate was 0.245 m below the nozzle, and consequently the droplet impact velocity was numerically simulated to be 4.5 m/s and the droplet impact temperature was numerically simulated to be 232 °C with 97% liquid.

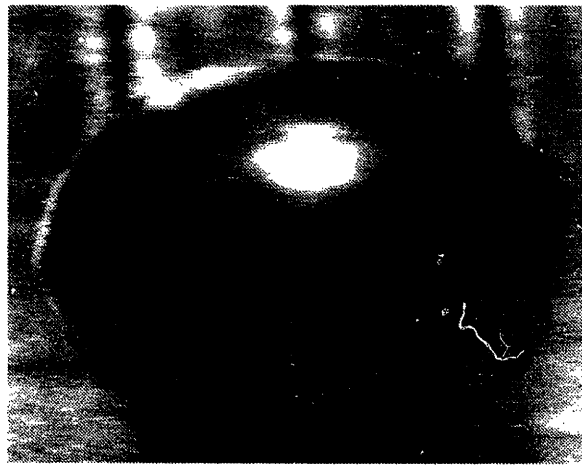
Figure 4.3 shows that the deposition rate plays a significant role in determining the shapes of deposits. Low frequency deposition produced a vertical pillar (Figure 4.3 (a)), whereas high frequency deposition resulted in a large drop (Figure 4.3 (b)). This work is in a qualitative agreement with the work of Gao and Sonin (1994) using wax droplets. They suggested that a vertical pillar be produced when the deposition frequency is so low that the tip of the pillar has enough time to solidify and cool before next droplet arrives. At high frequencies, there is insufficient time for droplets to cool down, and thus they coalesce into a large drop upon arrival. However, there is a quantitative discrepancy between this work and the work of Gao and Sonin because the thermal states of wax droplets are different from those of metal droplets and wax droplets do not spread as much as tin droplets do.

Table 4.1 Initial condition of droplet spray for the deposition experiment

Orifice Diameter (μm)	150
Melt Temperature (K)	573
Melt Material	pure tin
Ejection Pressure (Pa)	103
Vibration Frequency (kHz)	6.3
Charging Voltage (V)	394



(a)



(b)

Figure 4.3 Deposits at two Different Frequencies; (a) at 57 Hz and (b) at 574 Hz; the width between the grids is 1mm.

Chapter 5 CONCLUSIONS

This work addressed the feasibility of rapid prototyping using the UDS process. Methods of maintaining a straight and stable liquid metal jet were devised and tested. The changes include an auxiliary orifice mounting fixture and a new crucible bottom with a tightly-fitting orifice-pocket. Satisfactory jet behavior was observed using the new crucible bottom in many repeated experiments.

Upon achieving the stable and straight liquid metal jet generation, a droplet trajectory controller including a pair of deflection plates and a pulse generator was developed to precisely deliver droplets, at a specified frequency, onto a substrate. The degree of separation between deflected and un-deflected droplet streams was modeled and compared with experimental results. The comparison revealed that the actual degree of separation (or deflection) is greater than the prediction. Depositions employing the controller described above were conducted using a 99.9% pure tin (Sn) at different frequencies. Low frequency deposition at 57Hz produced a vertical pillar, whereas high frequency deposition at 574Hz resulted in a large drop.

BIBLIOGRAPHY

Abel, G. K., 1993, "Characterization of Droplet Flight Path and Mass Flux in Droplet-Based Manufacturing," S.M. Thesis, Department of Mechanical Engineering, MIT.

Chen, C.-A., 1996, "Droplet Solidification and Its Effects on Deposit Microstructure in the Uniform Droplet Spray Process," Ph.D. Thesis, Department of Mechanical Engineering, MIT.

Gao, F. and Sonin, A. A., 1994, "Precise Deposition of Molten Microdrops: the Physics of Digital Microfabrication," *Proceedings of the Royal Society of London, A*, vol. 444, pp. 533-554.

Incropera, F.P., and DeWitt, D.P., 1990, *Introduction to Heat Transfer*, 2nd Ed., John Wiley & Sons, New York, NY.

Kim, H.-Y., 1998, Private Communication.

Mathur, P., Apelian, D., and Lawley, A., 1989, "Analysis of the Spray Deposition Process," *Acta Metallurgica*, vol. 37, pp. 429-443.

Mulholland, J. A., Srivastava, R. K., and Wendt, J. O. L., 1988, "Influence of Droplet Spacing on Drag Coefficient in Nonevaporating, Monodisperse Streams," *AIAA Journal*, vol. 26, pp. 1231-1237.

Passow, C. H., 1992, "A Study of Spray Forming Using Uniform Droplet Sprays." S.M. Thesis, Department of Mechanical Engineering, MIT.

Yim, P., 1996, "The Role of Surface Oxidation in the Break-Up of Laminar Liquid Metal Jets," Ph.D. Thesis, Department of Mechanical Engineering, MIT.